



Concomitant evaluation of cardiovascular and cerebrovascular controls via Geweke spectral causality to assess the propensity to postural syncope

Alberto Porta^{1,2} · Francesca Gelpi¹ · Vlasta Bari^{1,2} · Beatrice Cairo¹ · Beatrice De Maria³ · Davide Tonon⁴ · Gianluca Rossato⁴ · Luca Faes⁵

Received: 18 March 2023 / Accepted: 5 July 2023 / Published online: 15 July 2023
© The Author(s) 2023

Abstract

The evaluation of propensity to postural syncope necessitates the concomitant characterization of the cardiovascular and cerebrovascular controls and a method capable of disentangling closed loop relationships and decomposing causal links in the frequency domain. We applied Geweke spectral causality (GSC) to assess cardiovascular control from heart period and systolic arterial pressure variability and cerebrovascular regulation from mean arterial pressure and mean cerebral blood velocity variability in 13 control subjects and 13 individuals prone to develop orthostatic syncope. Analysis was made at rest in supine position and during head-up tilt at 60°, well before observing presyncope signs. Two different linear model structures were compared, namely bivariate autoregressive and bivariate dynamic adjustment classes. We found that (i) GSC markers did not depend on the model structure; (ii) the concomitant assessment of cardiovascular and cerebrovascular controls was useful for a deeper comprehension of postural disturbances; (iii) orthostatic syncope appeared to be favored by the loss of a coordinated behavior between the baroreflex feedback and mechanical feedforward pathway in the frequency band typical of the baroreflex functioning during the postural challenge, and by a weak cerebral autoregulation as revealed by the increased strength of the pressure-to-flow link in the respiratory band. GSC applied to spontaneous cardiovascular and cerebrovascular oscillations is a promising tool for describing and monitoring disturbances associated with posture modification.

Keywords Vector autoregressive model · Heart rate variability · Arterial pressure · Blood flow · Baroreflex · Cerebral autoregulation · Head-up tilt · Postural syncope

1 Introduction

Regulatory mechanisms governed by the autonomic function have a profound impact on the spontaneous dynamics of cardiovascular and cerebrovascular variables and their relationships. Heart period (HP) is mainly under vagal control because atropine dramatically decreases HP variability [1], while sympathetic activation induced by an orthostatic stressor increases the magnitude of the systolic arterial pressure (SAP) fluctuations especially in the low frequency (LF) band [2, 3]. Sympathetic drive affects cerebrovascular circulation as well, even though the contribution of vagal circuits cannot be dismissed [4, 5]. Autonomic function influences the cardiac arm of the baroreflex, usually described by the dynamic relationship from SAP to HP [2, 6, 7], and cerebral autoregulation (CA), as inferred from the dynamic link from mean arterial pressure (MAP) to mean cerebral blood velocity (MCBv) [8, 9].

✉ Alberto Porta
alberto.porta@unimi.it

¹ Department of Biomedical Sciences for Health, University of Milan, 20133 Milan, Italy

² Department of Cardiothoracic, Vascular Anesthesia and Intensive Care, IRCCS Policlinico San Donato, Via R. Morandi 30, San Donato Milanese, 20097 Milan, Italy

³ IRCCS Istituti Clinici Scientifici Maugeri, 20138 Milan, Italy

⁴ Department of Neurology, IRCCS Sacro Cuore Don Calabria Hospital, 37024 Negrar, Verona, Italy

⁵ Department of Engineering, University of Palermo, 90128 Palermo, Italy

Model-based causality analysis [10, 11] applied to cardiovascular and cerebrovascular variability series is becoming a traditional tool in characterizing regulatory mechanisms [12, 13] aiming at stabilizing physiological variables such as arterial pressure (AP) and cerebral blood flow (CBF). Such an interest is linked to the ability of causality tools to quantify modifications of the strength of the causal link between two signals, one taken as a drive and the other as a target, occurring in response to a stimulus challenging cardiovascular and/or cerebrovascular homeostasis [14–23]. For example, the application of model-based causality analysis to cardiovascular variables suggests that orthostatic challenge increases the strength of the causal relationship from SAP to HP along the cardiac arm of the baroreflex in proportion to the magnitude of the stressor [15, 18, 24]. Model-based causality tools have been applied to describe cerebrovascular control as well: indeed, it was found that an orthostatic stressor increases the strength of the dependence of MCBv on MAP along the pressure-to-flow pathway only in individuals prone to develop postural syncope [19] thus suggesting the inability of the CA in limiting the variability of MCBv in response to MAP changes.

Some methodological key features of causality analysis are currently under scrutiny because they might have a profound impact on conclusions. First, it is still unclear whether model-based spectral causality analysis [25–33] provides additional insight compared to causal markers derived in time domain using Granger causality and/or transfer entropy [14–24]. Time domain causality approaches do not provide scale-specific information [14–24]. Conversely, physiological mechanisms operate in specific frequency bands: for example, baroreflex generates oscillations about its resonance frequency (i.e., about 0.1 Hz) [34, 35] and cerebrovascular mechanisms feature time scales even slower (i.e., from 0.02 to 0.07 Hz) [36]. Since spectral causality indexes could be made scale-specific by computing them in assigned frequency bands, those markers should be superior in describing the inherent functioning of physiological mechanisms compared to time domain causality indexes. Second, it is unclear whether the underlying model structure adopted to interpret causal relationships might have an impact on the conclusions. Model structures capable of describing rhythms that cannot be fully explained by dynamical interactions among signals, such as the dynamic adjustment model (DA) class, might provide some advantage with respect to model structures that do not have this possibility, such as the autoregressive model (AR) class [15, 27, 37, 38]. Third, it is unclear whether the concomitant analysis of cardiovascular and cerebrovascular variability interactions via spectral causality analysis might provide useful information in stratifying

the risk of syncope in patients prone to orthostatic intolerance during an orthostatic stressor.

The present study is specifically designed to address the three above-mentioned issues over a historical database utilized to assess cardiovascular and cerebrovascular variability interactions in subjects prone to develop postural syncope (SYNC) compared to control individuals who never experienced postural syncope (noSYNC) [19, 39, 40]. Geweke spectral causality (GSC) [11] was utilized to differentiate cardiovascular and cerebrovascular regulations in SYNC and noSYNC groups over variability series of SAP and HP and of MAP and MCBv using two different model structures, namely the bivariate AR (BAR) and the bivariate DA (BDA) classes. We hypothesize that GSC could provide additional information compared to a previous time domain causality analysis working regardless of time scales and applied to the same data [19], and that conclusions do not depend on the structure of the model utilized to describe dynamic interactions, namely BAR or BDA.

2 Experimental protocol and data analysis

2.1 Compliance with ethical standards

The study adhered to the principles of the Declaration of Helsinki for medical research involving humans. The protocol was approved by the ethical committee of the IRCCS Sacro Cuore Don Calabria Hospital, Negrar, Italy (protocol number: 101/2010; date of approval: 1/5/2010). All subjects provided written informed consent before entering the study.

2.2 Experimental protocol

Data were collected to explore the possibility of stratifying the risk of fainting via the analysis of spontaneous cardiovascular and cerebrovascular oscillations evoked by volume shift toward lower limbs induced by a postural stimulus [19, 39, 40]. In this study, we considered 13 SYNC subjects (age: 28 ± 9 years; 5 males) and 13 noSYNC control subjects (age: 27 ± 8 years; 5 males). The SYNC subjects were highly likely to faint because they had a history of syncope with more than 3 events/year in their last 2 years. This propensity was verified via prolonged head-up tilt protocol. Events were considered of unknown etiology because clinical and physical assessment excluded common causes linked to neurological, electrocardiographic, and hemodynamic factors. The health condition of noSYNC individuals was verified via similar clinical screening and the prolonged head-up tilt test certified their resistance to syncope.

Preparation of the subjects, characteristics of the facilities where experimental sessions took place, and instructions given to the subjects were reported in [39, 40]. SYNC and noSYNC individuals were free from any medication known to interfere with cardiovascular and/or cerebrovascular controls. We acquired the electrocardiogram (ECG) in a lead II configuration, volume-clamp continuous AP from the middle finger of the right hand (Finapres Medical Systems, Enschede, The Netherlands) and CB velocity (CBv) from the right or left middle cerebral artery via a transcranial Doppler device (Multi-Dop T, DWL, 2 MHz, Compumedics, San Juan Capistrano, CA, USA) [41]. CBv was considered a proxy of CBF under the hypothesis of negligible modifications of the vessel diameter [36]. All signals were sampled synchronously at 1000 Hz. Attention was paid to leave a period of stabilization of the physiological variables before starting the acquisition session. ECG, AP and CBv were recorded for 10 min with the subject lying at rest in horizontal position (REST) on the tilt table. Then, it was rotated to reach an inclination of 60° and recording session during head-up tilt (HUT) started. Tilt table rotated continuously from horizontal position to 60° in 15 s. If no signs of presyncope were observed during HUT, the duration of the session was prolonged up to 40 min. Otherwise, the subject was immediately returned to REST. As expected, presyncope signs were observed in all SYNC subjects at different timings, while HUT session lasted 40 min in noSYNC subjects. The syncope occurred after 1047 ± 546 s from the HUT onset in SYNC subjects.

2.3 Beat-to-beat variability series

The time interval between two consecutive R-wave peaks of the ECG was taken as the n th HP (HP_n). The maximum AP within HP_n was identified as the n th systolic AP (SAP_n). The n th diastolic arterial pressure (DAP_n) was the minimum of AP following SAP_n . Detections of R-wave peaks from the ECG and AP fiducial points were visually checked. Procedures to insert missed identifications, to correct and reinsert eventual misdetections and to limit the effect of arrhythmic beats were described in [39, 40]. Only few isolated ectopic beats were detected, and their number was always less than 5% of the total length of the sequence. The MAP_n was derived as the ratio of the definite integral of AP between the timing of DAP_{n-1} and DAP_n to the interdiastolic interval. $MCBv_n$ was calculated similarly using the same fiducial points for the computation of the definite integral over the CBv signal [40]. As the focus of the study was the characterization of short-term regulatory mechanisms, the analysis was carried out over sequences of 256 consecutive synchronous HP, SAP, MAP and MCBv values taken in a random position within REST and HUT sessions [36, 42]. Stationarity of mean and variance was checked as proposed in [43]. Transitory adjustments of the variables during the transition from REST to HUT were avoided. Regardless of

the group, the selection of HUT segments was carried out in the early phase of HUT (i.e., within the first 10 min) and before the observation of any presyncope sign in SYNC individuals. Time domain markers were reported in [44]. Briefly, HP and MCBv means decreased during HUT in both groups. HP variance declined during HUT compared to REST in SYNC group. At REST, MAP mean was smaller in SYNC compared to noSYNC and in SYNC increased during HUT compared to REST. SAP mean and SAP, MAP and MCBv variances did not change across groups and conditions.

2.4 Computation of GSC markers

The joint interactions between two stochastic processes Y_1 and Y_2 were described by the bivariate process $Y = [Y_1 \ Y_2]^T$, where T is the transposition operator. Y belongs to the class of BAR and BDA processes [27, 38]. BAR and BDA processes differ for the structure of the innovation $W = [W_1 \ W_2]^T$ whose components are Gaussian white noises in the case of BAR process and Gaussian AR noises in the case of BDA process [27, 38]. GSC evaluates the strength of the causal interactions from Y_i to Y_j with $i, j = 1, 2$ and $i \neq j$ as a function of the frequency f as the negative logarithm of the fractional contribution of the partial power spectral density of Y_j due W_j to the overall power spectral density of Y_j [11]. Indeed, this fractional contribution decreases toward 0, while increasing the importance of the pathway from Y_i to Y_j [11]. We refer to [45] for the complete derivation of GSC markers from partial power spectral densities estimated via BAR and BDA model coefficients.

GSC markers were computed with $Y_1 = HP$ and $Y_2 = SAP$ to describe the cardiovascular regulation and with $Y_1 = MCBv$ and $Y_2 = MAP$ to describe the cerebrovascular control. Analyses were carried out over normalized series with zero mean and unit variance. More specifically, normalization was carried out by estimating a linear regression over time in the original series and by subtracting the linear trend from the original data. Each sample of the resulting zero mean series was divided by the standard deviation to obtain a series with unit variance. Coefficients of the BAR model were identified via traditional least squares technique, while those of the BDA one via generalized least squares method [38]. Identification problem was solved via the Cholesky decomposition method. Generalized least squares method was stopped [38] if the absolute value of the fractional between-iteration decline of prediction error variance was below 0.001. The model order was optimized via the Akaike information criterion for multivariate processes [46] in the range from 7 to 12. The latency from SAP to HP was set to 0 beats and that from HP to SAP to 1 beat [24, 27]. The latency from MAP to MCBv was set to 2 beats and that from MCBv to MAP to 0 beats [23, 47]. Markers were computed by integrating the GSC functions

over frequency bands [11] set according to the functioning of the cardiovascular and cerebrovascular controls. For the analysis of HP-SAP variability interactions, we adopted the typical frequency bands utilized for the analysis of cardiovascular variability series [6, 42], namely the LF band from 0.04 to 0.15 Hz and the high frequency (HF) band from 0.15 to 0.4 Hz. For the analysis of MCBv-MAP variability interactions, we adopted the frequency bands utilized for the analysis of cerebrovascular variability series [36], namely the very low frequency (VLF) band from 0.02 to 0.07 Hz, LF band from 0.07 to 0.15 Hz and HF band from 0.15 to 0.4 Hz. The superior cut-off of the LF band and the inferior cut-off of the HF band were reduced to 0.15 Hz from the original suggestion [36] due to the possible presence of slow breathing rate in young individuals [47]. The GSC markers computed over HP and SAP in the LF band were denoted as $GSC_{SAP \rightarrow HP}(LF)$ and $GSC_{HP \rightarrow SAP}(LF)$, while those in the HF band as $GSC_{SAP \rightarrow HP}(HF)$ and $GSC_{HP \rightarrow SAP}(HF)$. The GSC markers computed over MCBv and MAP in the VLF band were denoted as $GSC_{MAP \rightarrow MCBv}(VLF)$ and $GSC_{MCBv \rightarrow MAP}(VLF)$, those in the LF band as $GSC_{MAP \rightarrow MCBv}(LF)$ and $GSC_{MCBv \rightarrow MAP}(LF)$, and those in the HF band as $GSC_{MAP \rightarrow MCBv}(HF)$ and $GSC_{MCBv \rightarrow MAP}(HF)$.

2.5 Testing the appropriateness of the model structure

We tested the null hypothesis that the model structure was appropriate by checking whether autocorrelation computed over the model residuals and cross-correlation computed between the residuals were negligible at lags different from 0 ($LAG \neq 0$) and whether cross-correlation between the residuals was insignificant at lag equal to 0 ($LAG = 0$). We exploited two portmanteau tests applied at $LAG = 0$ and $LAG \neq 0$, respectively. The tests were based on the observation that the distribution of the square root of N times the normalized autocorrelation, or cross-correlation, converges toward a standard Gaussian distribution. More specifically, in $LAG = 0$ test the null hypothesis of negligible cross-correlation at lag equal to zero was rejected if the absolute value of the normalized cross-correlation at zero lag was larger than a threshold set as 1.96 divided by square root of $N - p_o$, where p_o is the optimal model order. The acceptance of the null hypothesis indicated the suitability of the model structure at zero lag. In the $LAG \neq 0$ test the null hypothesis of negligible autocorrelation, or cross-correlation, at lags different from 0 was rejected if the absolute value of the normalized autocorrelation, or cross-correlation, at lags different from 0 was larger than a threshold set as 1.96 divided by square root of $N - p_o - l$, where l was the lag. The null hypothesis of uncorrelation was rejected if the number of lags at which the absolute values of autocorrelation,

or cross-correlation, was found to be above the threshold was larger than 2, being 2 the 5% of the total amount of computed autocorrelation, or cross-correlation, samples (i.e., with $1 \leq l \leq L$ with $L = 40$). The test was carried out separately over autocorrelation and cross-correlation. The acceptance of the null hypothesis indicated that both autocorrelation and cross-correlation remained limited, thus suggesting the suitability of the model structure at lags different from 0.

2.6 Testing the null hypothesis of uncoupling via isodistribution isospectral surrogates

We tested the null hypothesis of full uncoupling [13] between the two processes Y_1 and Y_2 via the construction of sets of surrogate pairs preserving the distribution and power spectral density of the original series [48] but being fully uncoupled [49]. This null hypothesis was tested by generating 100 realizations of Y_1 and Y_2 for each original pair in any given group and experimental condition. The surrogate series were built to preserve the distribution and power spectral density of the original series, while phases were substituted with uniformly distributed random numbers ranging from 0 to 2π . We exploited an iteratively refined amplitude-adjusted, Fourier transform-based procedure to generate surrogate pairs [48]. It allowed the exact preservation of the original distribution, while the power spectrum was the best approximation of the initial power spectrum given 100 iterates. The use of two independent random phase sequences allowed the generation of fully uncoupled pairs [49]. The length of the series (i.e., 256) allowed us to speed up the construction of surrogate set via fast Fourier transform procedure. GSC markers were computed over each set of surrogates and the 95th percentile was extracted. If the marker computed over the original series was above the 95th percentile of the GSC markers derived from surrogates, the null hypothesis of uncoupling was rejected and the alternative hypothesis, namely the series were significantly associated in the considered time direction, was accepted. The percentage of subjects with a significant HP-SAP coupling was monitored as well as the one with a significant MCBv-MAP coupling. These percentages were computed for each frequency band and labelled as $GSC_{SAP \rightarrow HP}(LF)\%$, $GSC_{HP \rightarrow SAP}(LF)\%$, $GSC_{SAP \rightarrow HP}(HF)\%$, $GSC_{HP \rightarrow SAP}(HF)\%$, $GSC_{MAP \rightarrow MCBv}(VLF)\%$, $GSC_{MCBv \rightarrow MAP}(VLF)\%$, $GSC_{MAP \rightarrow MCBv}(LF)\%$, $GSC_{MCBv \rightarrow MAP}(LF)\%$, $GSC_{MAP \rightarrow MCBv}(HF)\%$ and $GSC_{MCBv \rightarrow MAP}(HF)\%$.

2.7 Statistical analysis

Two-way repeated measures analysis of variance (one factor repetition, Holm-Sidak test for multiple comparisons) was utilized to assess the significance of the differences between

groups within the same experimental condition (i.e., REST or HUT) and between experimental conditions within the same group (i.e., SYNC or noSYNC). If hypotheses for the utilization of Holm-Sidak test were not fulfilled, nonparametric tests (i.e., Mann–Whitney rank sum and Wilcoxon signed rank tests) were applied when appropriate. The level of significance of each test was lowered according to the number of comparisons (i.e., 4) to account for the multiple comparison issue. The χ^2 test (McNemar’s test) was applied to the proportion of subjects featuring the rejection of the null hypothesis of uncoupling to assess the effect of HUT within the assigned group. Traditional χ^2 test was applied to check the different behavior of noSYNC and SYNC subjects within the same experimental condition. Even in this case the level of significance of the test was lowered according to the number of comparisons (i.e., 4) to account for the multiple comparison issue. The analysis over the proportion of subjects featuring the rejection of the null hypothesis of uncoupling was carried out after pooling together the results of surrogate data analysis relevant to BAR and BDA models. Statistical analysis was performed with a commercial statistical software (Sigmaplot v.14.0, Systat Software, San Jose, CA, USA). The level of statistical significance of all the tests was set to 0.05. A type-I error probability p smaller than the level of significance was always taken as significant.

3 Results

3.1 Results on cardiovascular control

The optimal model order p_o of the BAR and BDA structures describing HP-SAP dynamic interactions was reported in Table 1. p_o did not vary across groups and experimental conditions. The null hypothesis of negligible correlation between the residuals of HP and SAP at zero lag, tested via the $LAG=0$ test, was accepted in 100% of the subjects and this result held regardless of the model structure, experimental condition, and group. The null hypothesis of insignificant autocorrelation and cross-correlation within and between the residuals at lags different from 0, tested via the $LAG \neq 0$ test, was accepted in more than, or equal to, 69% of the subjects and this result held regardless of the model structure, experimental condition, and group (Table 2).

The grouped vertical box-and-whisker plots of Fig. 1 show $GSC_{SAP \rightarrow HP}(LF)$ (Fig. 1a), $GSC_{HP \rightarrow SAP}(LF)$ (Fig. 1b), $GSC_{SAP \rightarrow HP}(HF)$ (Fig. 1c) and $GSC_{HP \rightarrow SAP}(HF)$ (Fig. 1d) as a function of the experimental condition (i.e., REST and HUT) in SYNC individuals (white boxes) and noSYNC subjects (grey boxes). Markers were computed via the BAR model. The height of the box represents the distance between the first and third quartiles, with the median marked as a line, and the whiskers show

Table 1 Optimal model order p_o of BAR and BDA models describing the HP-SAP dynamical interactions

p_o	Experimental condition	SYNC	noSYNC
BAR	REST	8.1 ± 1.6	7.8 ± 1.2
	HUT	7.6 ± 0.9	8.3 ± 1.8
BDA	REST	7.7 ± 1.4	7.2 ± 0.6
	HUT	7.7 ± 1.4	7.8 ± 1.5

p_o , optimal model order; SYNC, subjects with a history of recurrent postural syncope; noSYNC, subjects without a history of recurrent postural syncope; HP, heart period; SAP, systolic arterial pressure; BAR, bivariate autoregressive model; BDA, bivariate dynamic adjustment model; REST, at rest in supine position; HUT, head-up tilt at 60°

Table 2 Percentage of acceptance of the null hypothesis of negligible autocorrelation and cross-correlation computed at lags different from 0 ($LAG \neq 0$) over the residuals of the BAR and BDA models describing the HP-SAP dynamical interactions

LAG \neq 0	Experimental condition	SYNC	noSYNC
BAR	REST	69	85
	HUT	77	77
BDA	REST	85	77
	HUT	92	92

SYNC, subjects with a history of recurrent postural syncope; noSYNC, subjects without a history of recurrent postural syncope; HP, heart period; SAP, systolic arterial pressure; BAR, bivariate autoregressive model; BDA, bivariate dynamic adjustment model; REST, at rest in supine position; HUT, head-up tilt at 60°

the 5th and 95th percentiles. $GSC_{SAP \rightarrow HP}(LF)$ increased during HUT in both SYNC and noSYNC groups, while no between-group difference was detected both at REST and during HUT (Fig. 1a). $GSC_{HP \rightarrow SAP}(LF)$ declined with HUT, but the decrease was significant only in noSYNC group, while it did not vary across groups either at REST or during HUT (Fig. 1b). The trends of $GSC_{HP \rightarrow SAP}(HF)$ (Fig. 1d) were like those of $GSC_{HP \rightarrow SAP}(LF)$ (Fig. 1b) but the decline with HUT was significant solely in the SYNC group. $GSC_{SAP \rightarrow HP}(HF)$ did not vary across either experimental conditions or groups (Fig. 1c).

Figure 2 has the same structure and shows the same indexes as Fig. 1, but the markers were computed via the BDA model. Trends with groups and experimental conditions are similar to those reported in Fig. 1 as well as the significance, thus suggesting that BAR and BDA models lead to the same conclusions.

The grouped bar graphs of Fig. 3 show $GSC_{SAP \rightarrow HP}(LF)\%$ (Fig. 3a), $GSC_{HP \rightarrow SAP}(LF)\%$ (Fig. 3b), $GSC_{SAP \rightarrow HP}(HF)\%$ (Fig. 3c) and $GSC_{HP \rightarrow SAP}(HF)\%$

Fig. 1 The grouped vertical box-and-whisker plots show $GSC_{SAP \rightarrow HP}(LF)$ (a), $GSC_{HP \rightarrow SAP}(LF)$ (b), $GSC_{SAP \rightarrow HP}(HF)$ (c) and $GSC_{HP \rightarrow SAP}(HF)$ (d) as a function of the experimental condition (i.e., REST and HUT). Indexes are computed in SYNC (white boxes) and noSYNC (grey boxes) subjects via the BAR model

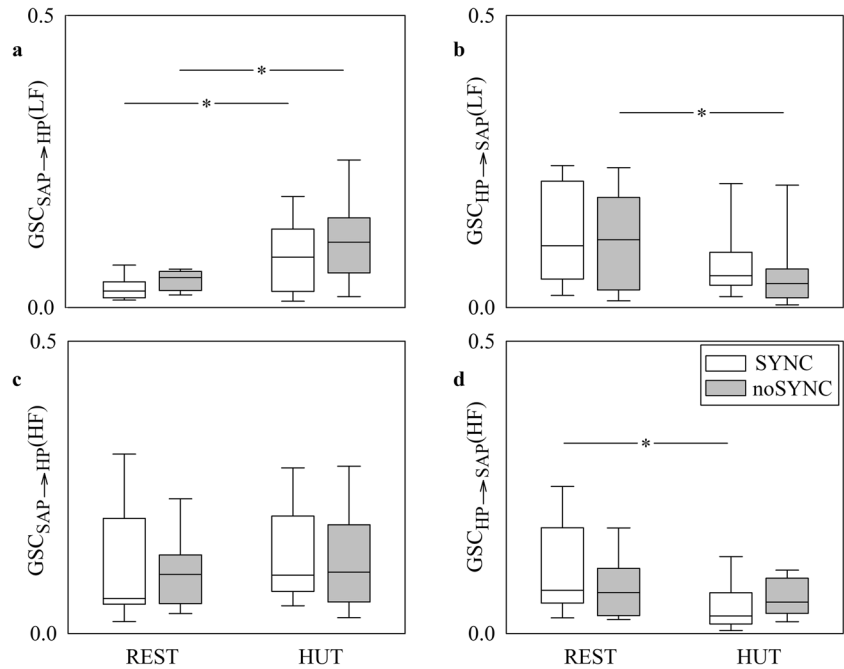


(Fig. 3d) as a function of the experimental condition (i.e., REST and HUT) in SYNC individuals (white bars) and noSYNC subjects (grey bars). The percentages were computed after pooling together the results of surrogate test based on BAR and BDA models given their similar performance as suggested by Fig. 1,2. $GSC_{SAP \rightarrow HP}(LF)\%$,

$GSC_{SAP \rightarrow HP}(HF)\%$ and $GSC_{HP \rightarrow SAP}(HF)\%$ did not vary across either experimental conditions or groups (Fig. 3a,c,d). $GSC_{HP \rightarrow SAP}(LF)\%$ decreased significantly in noSYNC compared to SYNC group solely during HUT, while the effect of HUT was not visible in either SYNC or noSYNC individuals (Fig. 3b).

Fig. 2 The grouped vertical box-and-whisker plots show $GSC_{SAP \rightarrow HP}(LF)$ (a), $GSC_{HP \rightarrow SAP}(LF)$ (b), $GSC_{SAP \rightarrow HP}(HF)$ (c) and $GSC_{HP \rightarrow SAP}(HF)$ (d) as a function of the experimental condition (i.e., REST and HUT). Indexes are computed in SYNC (white boxes) and noSYNC (grey boxes) subjects via the BDA model

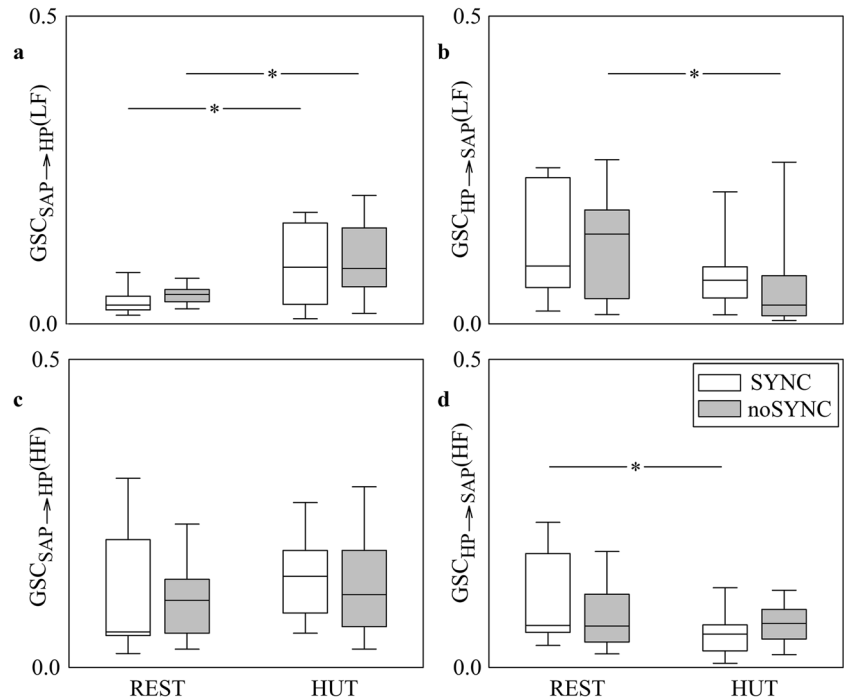


Fig. 3 The grouped vertical bar graphs show $GSC_{SAP \rightarrow HP}(LF)\%$ (a), $GSC_{HP \rightarrow SAP}(LF)\%$ (b), $GSC_{SAP \rightarrow HP}(HF)\%$ (c) and $GSC_{HP \rightarrow SAP}(HF)\%$ (d) as a function of the experimental condition (i.e., REST and HUT). Indexes are computed in SYNC (white bars) and noSYNC (grey bars) subjects. Percentages are computed by pooling together markers derived from both BAR and BDA models

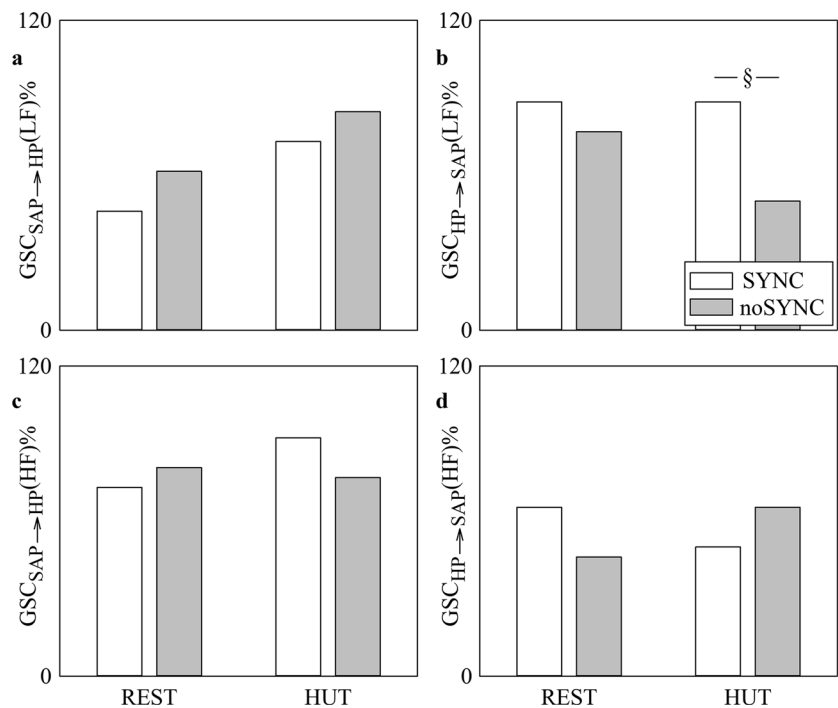


Table 3 Optimal model order p_o of BAR and BDA models describing the MCBv-MAP dynamical interactions

p_o	Experimental condition	SYNC	noSYNC
BAR	REST	8.2 ± 1.7	8.3 ± 1.4
	HUT	7.7 ± 1.2	8.7 ± 1.6
BDA	REST	7.7 ± 1.3	7.9 ± 1.4
	HUT	7.6 ± 1.5	8.5 ± 1.9

p_o , optimal model order; SYNC, subjects with a history of recurrent postural syncope; noSYNC, subjects without a history of recurrent postural syncope; MCBv, mean cerebral blood velocity; MAP, mean arterial pressure; BAR, bivariate autoregressive model; BDA, bivariate dynamic adjustment model; REST, at rest in supine position; HUT, head-up tilt at 60°

3.2 Results on cerebrovascular control

Table 3 shows the optimal model order p_o of the BAR and BDA structures describing MCBv-MAP dynamic interactions. p_o was not affected by HUT within the same group and remained unvaried in SYNC compared to noSYNC within the same experimental condition. The null hypothesis of negligible correlation between the residuals of MCBv and MAP at zero lag, tested via the LAG = 0 test, was accepted in 100% of the subjects and this result held regardless of the model structure, experimental condition, and group. The null hypothesis of insignificant autocorrelation and cross-correlation within and between the

Table 4 Percentage of acceptance of the null hypothesis of negligible autocorrelation and cross-correlation computed at lags different from 0 (LAG ≠ 0) over the residuals of the BAR and BDA models describing the MCBv-MAP dynamical interactions

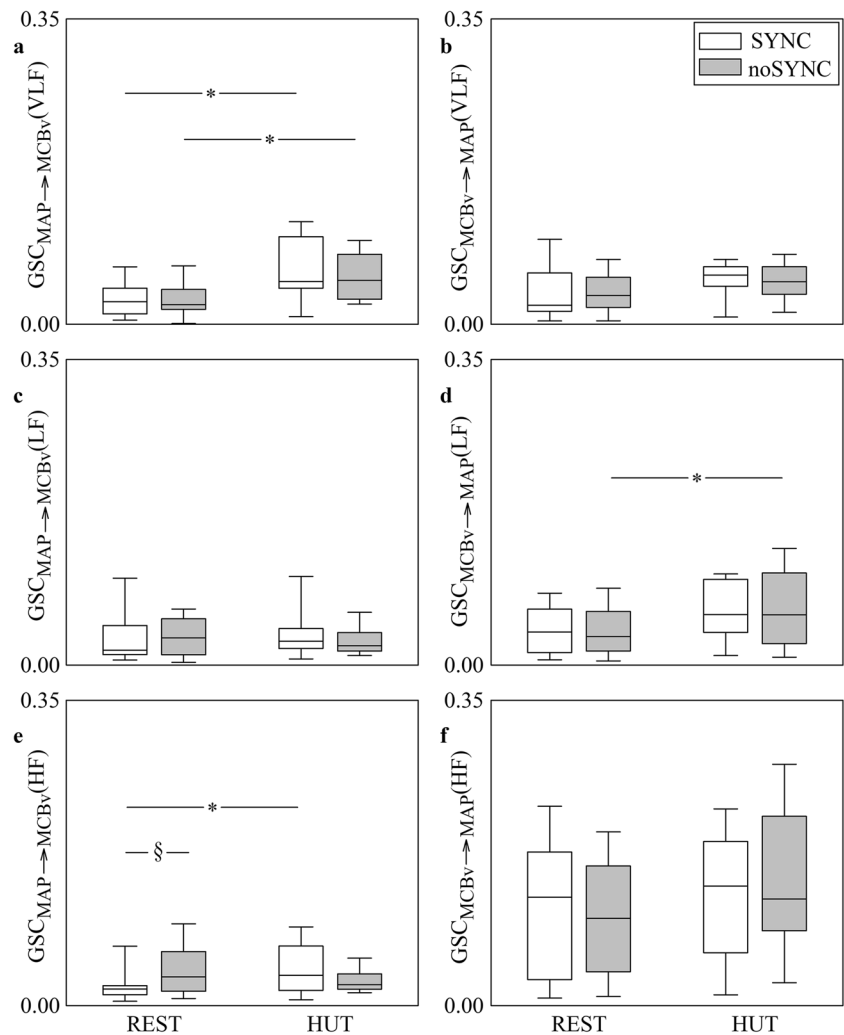
LAG ≠ 0	Experimental condition	SYNC	noSYNC
BAR	REST	62	85
	HUT	62	69
BDA	REST	85	85
	HUT	69	92

SYNC, subjects with a history of recurrent postural syncope; noSYNC, subjects without a history of recurrent postural syncope; MCBv, mean cerebral blood velocity; MAP, mean arterial pressure; BAR, bivariate autoregressive model; BDA, bivariate dynamic adjustment model; REST, at rest in supine position; HUT, head-up tilt at 60°

residuals at lags different from 0, tested via the LAG ≠ 0 test, was accepted in more than, or equal to, 62% of the subjects and this result held regardless of the model structure, experimental condition, and group (Table 4).

The grouped vertical box-and-whisker plots of Fig. 4 show $GSC_{MAP \rightarrow MCBv}(VLF)$ (Fig. 4a), $GSC_{MCBv \rightarrow MAP}(VLF)$ (Fig. 4b), $GSC_{MAP \rightarrow MCBv}(LF)$ (Fig. 4c), $GSC_{MCBv \rightarrow MAP}(LF)$ (Fig. 4d), $GSC_{MAP \rightarrow MCBv}(HF)$ (Fig. 4e) and $GSC_{MCBv \rightarrow MAP}(HF)$ (Fig. 4f) as a function of the experimental condition (i.e., REST and HUT) in SYNC individuals (white boxes) and noSYNC subjects (grey boxes). Markers were computed via the BAR model. The format of any box-and-whisker plot is the same as those in Fig. 1. $GSC_{MAP \rightarrow MCBv}(VLF)$ increased

Fig. 4 The grouped vertical box-and-whisker plots show $GSC_{MAP \rightarrow MCBv}(VLF)$ (a), $GSC_{MCBv \rightarrow MAP}(VLF)$ (b), $GSC_{MAP \rightarrow MCBv}(LF)$ (c), $GSC_{MCBv \rightarrow MAP}(LF)$ (d), $GSC_{MAP \rightarrow MCBv}(HF)$ (e) and $GSC_{MCBv \rightarrow MAP}(HF)$ (f) as a function of the experimental condition (i.e., REST and HUT). Indexes are computed in SYNC (white boxes) and noSYNC (grey boxes) subjects via the BAR model



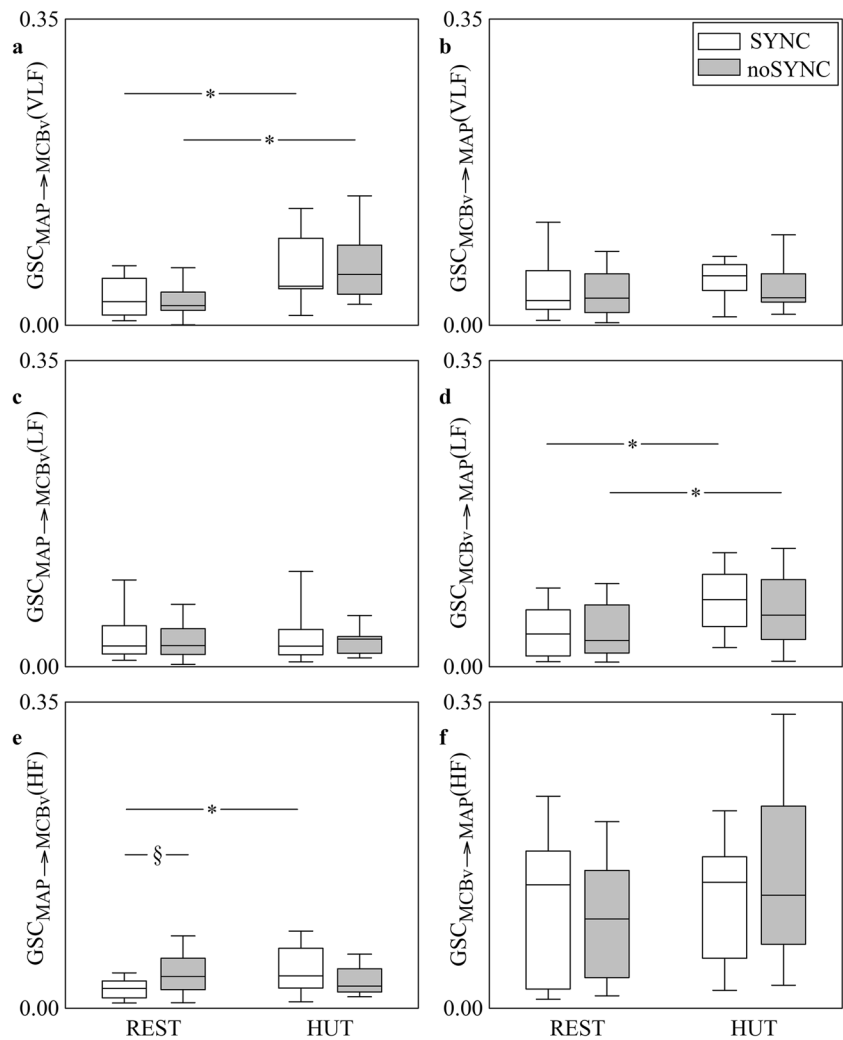
during HUT in both SYNC and noSYNC groups, while no between-group differences were detected both at REST and during HUT (Fig. 4a). $GSC_{MCBv \rightarrow MAP}(LF)$ increased during HUT compared to REST solely in noSYNC and the two groups were similar regardless of the experimental condition (Fig. 4d). At REST $GSC_{MAP \rightarrow MCBv}(HF)$ was higher in noSYNC compared to SYNC individuals, while it was similar in the two groups during HUT (Fig. 4e). Postural challenge raised $GSC_{MAP \rightarrow MCBv}(HF)$ solely in SYNC subjects (Fig. 4e). $GSC_{MCBv \rightarrow MAP}(VLF)$, $GSC_{MAP \rightarrow MCBv}(LF)$ and $GSC_{MCBv \rightarrow MAP}(HF)$ did not vary across either experimental conditions or groups (Fig. 4b,c,f).

Figure 5 has the same structure and shows the same indexes as Fig. 4, but the markers were computed via the BDA model. Trends with groups and experimental conditions are similar to those reported in Fig. 4. The sole additional significance compared to Fig. 4 is the increase of $GSC_{MCBv \rightarrow MAP}(LF)$ during HUT in SYNC group

(Fig. 5d). Comparison between Fig. 4 and Fig. 5 suggests that BAR and BDA models lead to the same conclusions.

The grouped bar graphs of Fig. 6 show $GSC_{MAP \rightarrow MCBv}(VLF)\%$, $GSC_{MCBv \rightarrow MAP}(VLF)\%$, $GSC_{MAP \rightarrow MCBv}(LF)\%$, $GSC_{MCBv \rightarrow MAP}(LF)\%$, $GSC_{MAP \rightarrow MCBv}(HF)\%$ and $GSC_{MCBv \rightarrow MAP}(HF)\%$ as a function of the experimental condition (i.e., REST and HUT) in SYNC individuals (white bars) and noSYNC subjects (grey bars). The percentages were computed after pooling together the results of surrogate test based on BAR and BDA models given their similar performance as suggested by Figs. 4,5. $GSC_{MAP \rightarrow MCBv}(VLF)\%$, $GSC_{MCBv \rightarrow MAP}(VLF)\%$, $GSC_{MAP \rightarrow MCBv}(LF)\%$ and $GSC_{MCBv \rightarrow MAP}(HF)\%$ did not vary across either experimental conditions or groups (Fig. 6a,b,c,f). $GSC_{MCBv \rightarrow MAP}(LF)\%$ and $GSC_{MAP \rightarrow MCBv}(HF)\%$ increased during HUT solely in SYNC but they did not separate groups either at REST or during HUT (Fig. 6d,e).

Fig. 5 The grouped vertical box-and-whisker plots show $GSC_{MAP \rightarrow MCBv}(VLF)$ (a), $GSC_{MCBv \rightarrow MAP}(VLF)$ (b), $GSC_{MAP \rightarrow MCBv}(LF)$ (c), $GSC_{MCBv \rightarrow MAP}(LF)$ (d), $GSC_{MAP \rightarrow MCBv}(HF)$ (e) and $GSC_{MCBv \rightarrow MAP}(HF)$ (f) as a function of the experimental condition (i.e., REST and HUT). Indexes are computed in SYNC (white boxes) and noSYNC (grey boxes) subjects via the BDA model



4 Discussion

The main findings of the study can be summarized as follows: (i) since the GSC approach can decompose the causal relationship in the frequency domain, it is particularly suitable for describing the frequency-dependent behavior of cardiovascular and cerebrovascular control mechanisms; (ii) tests carried out over residuals indicate that the model structures are suitable to describe dynamic interactions and results of the GSC analysis do not depend on the structure of the model; (iii) the development of syncope in SYNC group appear to be favored by the loss of coordinated behavior between baroreflex feedback and mechanical feedforward pathway in the frequency band typical of the AP regulation (i.e., the LF band) more than by a derangement of the baroreflex; (iv) SYNC group features a weaker CA compared to noSYNC subjects as revealed by the increased MCBv-MAP association along the pressure-to-flow link in the HF band during HUT; (v) taking all the findings together we suggest that the concomitant assessment of cardiovascular

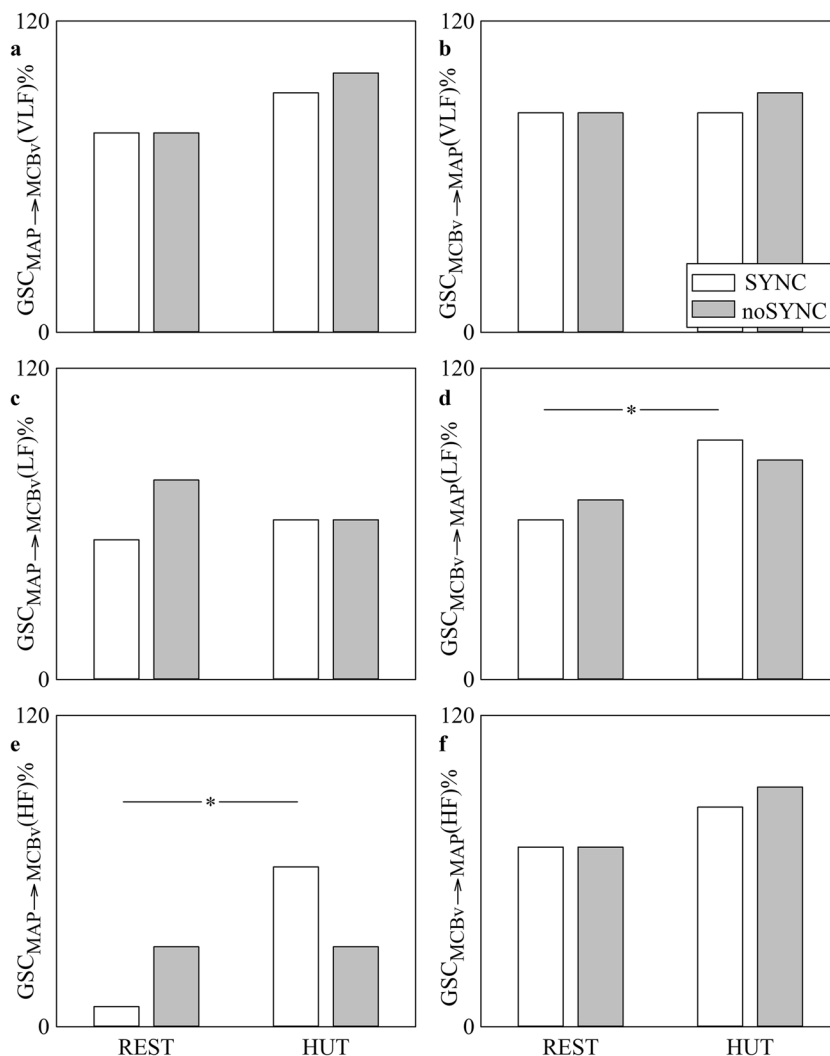
and cerebrovascular controls via a GSC approach can provide a more complete picture of the complexity of the physiological mechanisms leading to postural syncope.

4.1 GSC provides a frequency domain decomposition of the strength of the cardiovascular and cerebrovascular causal links

The most important feature of the GSC analysis is the possibility of decomposing the strength of the causal link into contributions at given frequencies that, when summed up, provide the overall contribution in a frequency band. This feature is particularly important in cardiovascular and cerebrovascular regulations given that physiological control mechanisms are frequency-dependent.

At the level of cardiovascular control, the sinus node transfer function has a low pass filter characteristic with a much lower corner frequency when fed by fluctuations of sympathetic tone than vagal activity [50], thus leading to heart rate

Fig. 6 The grouped vertical bar graphs show $GSC_{MAP \rightarrow MCBv}(VLF)\%$ (a), $GSC_{MCBv \rightarrow MAP}(VLF)\%$ (b), $GSC_{MAP \rightarrow MCBv}(LF)\%$ (c), $GSC_{MCBv \rightarrow MAP}(LF)\%$ (d), $GSC_{MAP \rightarrow MCBv}(HF)\%$ (e) and $GSC_{MCBv \rightarrow MAP}(HF)\%$ (f) as a function of the experimental condition (i.e., REST and HUT). Indexes are computed in SYNC (white bars) and noSYNC (grey bars) subjects. Percentages are computed by pooling together markers derived from both BAR and BDA models



fluctuations with negligible contribution of the sympathetic control above 0.15 Hz and concomitant contributions of both branches of the autonomic nervous system (ANS) below 0.15 Hz [1]. The transfer function from respiration to heart rate has different properties according to the state of the ANS with a steeper role-off in situation of sympathetic overactivity and a wider bandwidth in supine resting condition [51]. Baroreflex, namely the pathway from SAP to HP, comprises a fast vagal arm and a slower branch, more under sympathetic regulation [52]. The bandwidth of the baroreflex depends on the ANS state being much more limited in situations of sympathetic activation [7]. The functioning of the link from HP to SAP varies with frequency as well, given that it lumps together Windkessel effect and Frank-Starling law [34] that depend on frequency-optimized neural controls of peripheral resistances and ventricular contractility [53, 54].

Even at the level of the cerebrovascular control, the frequency-dependent behavior of the MCBv-MAP relationship is well-known. Indeed, the link from MAP to MCBv was usually modelled as a high-pass filter in the range of

frequencies of cerebrovascular variability (i.e., from 0.02 to 0.3 Hz) [55]. The autonomic control importantly modifies the frequency response of this filter. In fact, along the pressure-to-flow link ganglionic blockade increased the MCBv-MAP transfer function gain and reduced phase lead of MCBv to MAP variations [8], thus suggesting the important contribution of sympathetic control to CA. The frequency-dependent role of sympathetic regulation on cerebrovascular variability was also suggested by the increase of the MCBv-MAP transfer function gain above 0.05 Hz after α -adrenergic blockade [4]. Remarkably, this influence is extended to the reverse causal directions as well, namely to the flow-to-pressure link, commonly referred to as Cushing reflex [56], given that α 1-adrenergic blockade reduced the strength of the association from MCBv to MAP [21]. However, it is worth stressing that the frequency-dependent characteristic of cerebrovascular regulation is not the exclusive consequence of sympathetic control given the important influence of the cholinergic modulation on the MCBv-MAP transfer function above 0.04 Hz [5].

4.2 On the suitability and interchangeability of BAR and BDA model structures

We compared two linear regression models, namely BAR and BDA, widely utilized in the field of the evaluation of cardiovascular and cerebrovascular controls [7, 15, 19, 21, 23, 27, 32, 34, 35, 38, 57–64]. The two models differ for the description of the disturbance corrupting the target signal [15, 27, 37, 38]: in the BAR model the disturbing influence is modelled as a white noise, while in the BDA model, it is an AR process. Therefore, BDA is usually preferred when it could be hypothesized that some oscillatory mechanisms of unknown origin act on the target without being explained by either self- or cross-dependencies [15, 27, 37, 38], such as the activity of the respiratory centers driving HP via direct modulation of vagal outflow [65] or movements of cerebrospinal fluid driven by respiratory modulations of intrathoracic pressure capable of modifying MCBv even in the presence of stable MAP via changes of intracranial pressure [66]. Both the model structures are suitable for describing cardiovascular and cerebrovascular dynamic interactions given that the hypotheses of whiteness of the residuals and their uncorrelation, even at zero lag, was fulfilled in most of the subjects. In addition, we found that results of GSC did not depend on the structure of the model. This finding suggests that BAR is sufficient for the purpose of describing spectral contents of the causal relationships in the context of bivariate analysis. However, this result might not hold for a multivariate approach.

4.3 SYNC group features a loss of coordinated behavior between the baroreflex and mechanical feedforward pathway in the LF band

Previous studies exploiting causality indexes operating over the entire range of time scales suggested that cardiovascular control in SYNC and noSYNC subjects exhibited different responses to HUT [19]. Indeed, while the strength of the causal relationship from SAP to HP along baroreflex increased in noSYNC individuals [15, 18, 24], postural stressor did not activate the baroreflex in SYNC subjects [19], thus suggesting an impairment of the cardiac arm of baroreflex in this group that might be mediated by a more prolonged latency [67]. The present study makes more specific the original observation reported in [19]. Indeed, the increased strength of the dependence of HP on SAP along baroreflex during HUT was observed solely in the LF band, thus confirming that baroreflex control operates more importantly in this frequency band [6, 34, 35]. An effect of the HUT over the mechanical feedforward pathway was evident as well: it took the form of a decreased strength of

the link from HP to SAP in the LF band, thus suggesting the decreased importance of this pathway with respect to the baroreflex one during HUT [24]. Remarkably, this effect over the mechanical feedforward link was significant only in noSYNC individuals, thus suggesting the balance between increased strength along the baroreflex and the decreased coupling along the mechanical feedforward is important to present postural intolerance. In the HF band, HUT did not affect the degree of association from SAP to HP and marginally influenced the one on the reverse causal relationship. Our analysis could detect between-group differences as well. Remarkably, the two groups were not separated at the level of the involvement of baroreflex in governing causal dynamic interactions from SAP to HP, as it could be expected whether SYNC group exhibited a baroreflex impairment as suggested in [19]. Conversely, the relevant role of the mechanical feedforward pathway was stressed during HUT by the lower percentage of noSYNC individuals with a significant degree of coupling from HP to SAP in the LF band compared to the SYNC ones. This differentiation between the two population was not obtained using time domain casualty methods in [19], thus suggesting GSC might be more powerful in typifying the derangement of cardiovascular control than time domain causality markers. Indeed, we interpret the limited responsiveness of the baroreflex to the postural challenge observed in SYNC group detected in [19] as the result of much greater constancy of the strength from HP to SAP in the LF band preventing the identification of the activation of baroreflex in this population.

4.4 SYNC group features a weaker CA in the HF band

The analysis of cerebrovascular control in SYNC and noSYNC subjects via causality markers that operate over the entire range of time scales suggested that the two groups exhibited different responses to HUT [19]. Indeed, while the strength of the causal relationship from MAP to MCBv remained unvaried during HUT in noSYNC individuals, it increased in SYNC individuals [19]. This finding was interpreted as a sign of the impairment of CA in the SYNC group because a working CA should limit the association between MAP and MCBv variability such a way to prevent MAP modifications to drive MCBv changes [9, 19, 68]. This study confirmed this finding and made it much more specific due to the ability of the present approach to separate frequency bands. Indeed, the strength of the pressure-to-flow dependence increased during HUT only in SYNC group in the HF band, leading to an augmentation of the percentage of SYNC subjects with a significant coupling from MAP to MCBv. The weaker level of association from MAP to MCBv at

REST in SYNC group compared to noSYNC subjects is central for the detection of the significant increase during HUT in SYNC subjects, thus stressing that the healthy degree of MAP-MCBv coupling should not necessarily be too low or fully insignificant. Remarkably, SYNC and noSYNC groups exhibited different strengths of the causal link from MAP to MCBv just at REST, thus allowing us to hypothesize a structural difference of the cerebrovascular control between the two populations. It is worth noting that this result was reached in the absence of any difference between variability of MAP and MCBv and similar values of CA markers [44]. This peculiar result is evident along the pressure-to-flow link solely in the HF band: indeed, the strength of the pressure-to-flow dependence remained unvaried across groups and experimental conditions in the LF band and did not exhibit between-group difference in the VLF band. This finding might support the relevance of respiration [23] in checking the propensity to faint in SYNC group. The relevance of assessing the pressure-to-flow relationship in the HF band stresses the need to standardize tests to verify the ability of CA to limit the degree of association between MAP and MCBv in correspondence of a forcing input such as respiration. The effect of HUT was evident along the flow-to-pressure link as well. Remarkably, it was more evident in the LF band in agreement with the observation that this pathway is under sympathetic control [21].

4.5 On the relevance of the concomitant assessment of cardiovascular and cerebrovascular controls via a GSC approach

The most striking result of the simultaneous analysis of cardiovascular and cerebrovascular controls is that the differentiation between the two populations occurred at different time scales. While at the level of the cardiovascular variability interactions markers in the LF band during HUT led to the separation of the SYNC from noSYNC group, at the level of cerebrovascular variability the between-group disjunction was achieved in the HF band at REST. This finding leads us to hypothesize that respiratory input in control condition might be sufficient to unveil the impairment at the level of cerebrovascular control, while testing the efficiency of cardiovascular regulation requires a challenge empowering LF oscillations of baroreflex origin such as HUT. The present study stresses the critical role of the missed coordination between mechanical feedforward pathway and baroreflex feedback in cardiovascular control in the frequency band including the resonance frequency of the baroreflex loop (i.e., 0.1 Hz) and indicates the possible contribution of a dysregulated MCBv response to respiratory fluctuations of MAP as factors promoting the susceptibility of SYNC group to postural failure. These findings support the conclusion

that the sole assessment of either cardiovascular or cerebrovascular control might be insufficient to probe the complexity of the physiological regulations because it could provide a limited view on the system functioning. In addition, since this conclusion held only in specific frequency bands, being different in cardiovascular and cerebrovascular dynamic interactions, the application of a GSC method becomes mandatory because causality approaches in time domain working regardless of time scales cannot be useful at this regard.

The concomitant assessment of cardiovascular and cerebrovascular controls might be particularly relevant in studying postural intolerance disturbances. Postural syncope is an extremely debilitating problem experienced by subjects with a derangement of the autonomic control and even by healthy individuals after bed rest or spaceflight. Postural syncope occurs in response to a cerebral hypoperfusion secondary to a systemic hemodynamic failure. While the final event is the drop of cerebral perfusion, it is unclear whether an impairment of CA could contribute to syncope by exacerbating a CBF decline associated to a critical hemodynamic status or by even triggering a degeneration of an original hemodynamic situation that per se would not lead to hypoperfusion and consequent loss of consciousness. One of the factors that might contribute to a reduced brain perfusion during orthostatic challenge is the sympathetic activation induced by a change of posture [2, 3, 69, 70]: indeed, vasoconstriction at peripheral level, aiming at preserving venous return and cardiac output, reduces CBv at the level of brain circulation [9, 44, 71–73]. The contemporaneous analysis of cardiovascular and cerebrovascular controls might provide the correct perspective to elucidate the temporal sequence of events leading to the development of postural syncope. In addition, the application of a tool capable of describing closed loop relationships could assure a more insightful characterization of the involved mechanisms. Indeed, the separation of the effects of baroreflex feedback [6] from those of the mechanical feedforward pathway [34] in the cardiovascular control loop and the disconnection of the influences of the pressure-to-flow link [74] from those of the Cushing reflex [56] in the cerebrovascular control loop might favor the comprehension of mechanisms underlying postural syncope. In addition, since the GSC operates in different frequency bands and the effect of ANS over the cardiovascular and cerebrovascular regulatory loops is frequency-dependent, the possibility of accounting for time scales might be an additional advantage.

4.6 Limitations of the study and future developments

The present study SYNC and noSYNC groups were age- and gender-matched. Therefore, age and gender are not expected to have played a role on conclusions of the present study. However, since cardiovascular control depends on age and

gender [75–78] and a relationship between cardiovascular and cerebrovascular regulations has been observed [79, 80], future studies should investigate the dependence of spectral causality indexes on gender and age. Additional reflexes known to be activated by a maneuver inducing central hypovolemia could have contributed to the conclusions of this study. Among these reflexes, we mention the sympathetic and vascular resistance arms of the baroreflex [81–83], the control of cardiac contractility and stroke volume [83–86], the dynamical response of the leg muscles to AP changes [87–90] and cardiorespiratory interactions responsible for the direct effect of respiration on HP [90–92]. Future studies should be focused on accounting for confounding factors via the acquisition of additional series and extension of GSC methods to the multivariate case [31, 32]. In the present study, we applied two portmanteau's tests for checking the adequacy of the fitting carried out by the model. Instead of the application of portmanteau's tests, the Durbin-Watson test might be applied. Future studies could compare the two methods for testing significance of the autocorrelation of residuals and cross-correlation between residuals to check whether discrepancies between conclusions derived from the two statistical approaches could be detected.

5 Conclusions

Postural syncope propensity can be studied by applying GSC to the spontaneous fluctuations of physiological variables. The advantage of the GSC approach is to decompose in the frequency domain the strength of causal links along the two arms of the closed loop relationship. The technique was applied to the assessment of cardiovascular and cerebrovascular controls accounting for the dynamical interactions between HP and SAP and between MAP and MCBv respectively in subjects prone to develop postural syncope. Decomposition was carried out in specific frequency bands typical of the functioning of the mechanisms governing HP-SAP and MCBv-MAP variability interactions. Frequency decomposition of causal links, analysis of both the arms of the closed loop relationship, and concomitant assessment of cardiovascular and cerebrovascular controls were found to be helpful to describe the mechanisms that lead to orthostatic syncope. More specifically, we found that the postural syncope is favored by a loss of coordination between baroreflex feedback and mechanical feedforward pathway in response to HUT in the LF band and by a weaker ability of CA to limit MCBv variability driven by MAP changes at the respiratory rate during HUT. We advocate the use of the proposed approach to clarify the primary origin of postural syncope and precipitating factors, provide an early detection of people at risk of developing syncope, improve classification of patients according to the pattern of response to an

imposed stressor, test the effect of possible countermeasures, and monitor the sequence of events leading to the loss of consciousness.

Author contribution A.P.: Conceptualization, Methodology, Software, Validation, Formal Analysis, Data Curation, Resources, Writing—Original draft preparation, Writing—Review & Editing, Visualization, Supervision, Project Administration, Funding Acquisition. F.G., V.B., B.C., B.D.M.: Data Curation, Writing—Review & Editing. D.T., G.R.: Resources, Investigation, Data Curation, Writing—Review & Editing. L.F.: Writing—Review & Editing.

Funding Open access funding provided by Università degli Studi di Milano within the CRUI-CARE Agreement. The Italian Ministry of Health partially supported this study via Ricerca Corrente program to Policlinico San Donato.

Data availability The datasets used in the present study are available from the corresponding author on reasonable request.

Declarations

Competing interests The authors declare no competing interests.

Open Access This article is licensed under a Creative Commons Attribution 4.0 International License, which permits use, sharing, adaptation, distribution and reproduction in any medium or format, as long as you give appropriate credit to the original author(s) and the source, provide a link to the Creative Commons licence, and indicate if changes were made. The images or other third party material in this article are included in the article's Creative Commons licence, unless indicated otherwise in a credit line to the material. If material is not included in the article's Creative Commons licence and your intended use is not permitted by statutory regulation or exceeds the permitted use, you will need to obtain permission directly from the copyright holder. To view a copy of this licence, visit <http://creativecommons.org/licenses/by/4.0/>.

References

1. Pomeranz B, Macaulay RJ, Caudill MA, Kutz I, Adam D, Gordon D et al (1985) Assessment of autonomic function in humans by heart rate spectral analysis. *Am J Physiol* 248:H151–H153
2. Cooke WH, Hoag JB, Crossman AA, Kuusela TA, Tahvanainen KUO, Eckberg DL (1999) Human responses to upright tilt: a window on central autonomic integration. *J Physiol* 517:617–628
3. Marchi A, Bari V, De Maria B, Esler M, Lambert E, Baumert M et al (2016) Calibrated variability of muscle sympathetic nerve activity during graded head-up tilt in humans and its link with noradrenaline data and cardiovascular rhythms. *Am J Physiol* 310:R1134–R1143
4. Hamner JW, Tan CO, Lee K, Cohen MA, Taylor JA (2010) Sympathetic control of the cerebral vasculature in humans. *Stroke* 41:102–109
5. Hamner JW, Tan CO, Tzeng Y-C, Taylor JA (2012) Cholinergic control of the cerebral vasculature in humans. *J Physiol* 590(24):6343–6352
6. Laude D, Elghozi J-L, Girard A, Bellard E, Bouhaddi M, Castiglioni P et al (2004) Comparison of various techniques used to estimate spontaneous baroreflex sensitivity (the EuroBaVar study). *Am J Physiol* 286:R226–R231

7. Porta A, Gelpi F, Bari V, Cairo B, De Maria B, Takahashi ACM et al (2023) Changes of the cardiac baroreflex bandwidth during postural challenges. *Am J Physiol* 324:R601–R612
8. Zhang R, Zuckerman JH, Iwasaki K, Wilson TE, Crandall CG, Levine BD (2002) Autonomic neural control of dynamic cerebral autoregulation in humans. *Circulation* 106:1814–1820
9. Zhang R, Zuckerman JH, Levine BD (1998) Deterioration of cerebral autoregulation during orthostatic stress: insights from the frequency domain. *J Appl Physiol* 85:1113–1122
10. Granger CWJ (1980) Testing for causality. A personal viewpoint. *J Econ Dyn Control* 2:329–352
11. Geweke J (1982) Measurement of linear dependence and feedback between multiple time series. *J Amer Stat Assoc* 77:304–313
12. Porta A, Faes L (2013) Assessing causality in brain dynamics and cardiovascular control. *Phil Trans R Soc A* 371:20120517
13. Porta A, Faes L (2016) Wiener-Granger causality in network physiology with applications to cardiovascular control and neuroscience. *Proc IEEE* 104:282–309
14. Porta A, Bassani T, Bari V, Pinna GD, Maestri R, Guzzetti S (2012) Accounting for respiration is necessary to reliably infer Granger causality from cardiovascular variability series. *IEEE Trans Biomed Eng* 59:832–841
15. Porta A, Bassani T, Bari V, Tobaldini E, Takahashi ACM, Catai AM et al (2012) Model-based assessment of baroreflex and cardiopulmonary couplings during graded head-up tilt. *Comput Biol Med* 42:298–305
16. Porta A, Castiglioni P, Di Rienzo M, Bassani T, Bari V, Faes L et al (2013) Cardiovascular control and time domain Granger causality: insights from selective autonomic blockade. *Phil Trans R Soc A* 371:20120161
17. Porta A, Faes L, Marchi A, Bari V, De Maria B, Guzzetti S et al (2015) Disentangling cardiovascular control mechanisms during head-down tilt via joint transfer entropy and self-entropy decompositions. *Front Physiol* 6:301
18. Porta A, Faes L, Nollo G, Bari V, Marchi A, De Maria B et al (2015) Conditional self-entropy and conditional joint transfer entropy in heart period variability during graded postural challenge. *PLoS ONE* 10:e0132851
19. Bari V, De Maria B, Mazzucco CE, Rossato G, Tonon D, Nollo G et al (2017) Cerebrovascular and cardiovascular variability interactions investigated through conditional joint transfer entropy in subjects prone to postural syncope. *Physiol Meas* 38:976–991
20. Javorka M, Czipelova B, Turianikova Z, Lazarova Z, Tonhajzerova I, Faes L (2017) Causal analysis of short-term cardiovascular variability: state-dependent contribution of feedback and feedforward mechanisms. *Med Biol Eng Comput* 55:179–190
21. Saleem S, Teal PD, Howe CA, Tymko MM, Ainslie PN, Tzeng Y-C (2018) Is the Cushing mechanism a dynamic blood pressure-stabilizing system? Insights from Granger causality analysis of spontaneous blood pressure and cerebral blood flow. *Am J Physiol* 315:R484–R495
22. Corbier C, Chouchou F, Roche F, Pichot B-C, V, (2020) Causal analyses to study autonomic regulation during acute head-out water immersion, head-down tilt and supine position. *Exp Physiol* 105:1216–1222
23. Porta A, Gelpi F, Bari V, Cairo B, De Maria B, Tonon D et al (2022) Categorizing the role of respiration in cardiovascular and cerebrovascular variability interactions. *IEEE Trans Biomed Eng* 69:2065–2076
24. Porta A, Catai AM, Takahashi ACM, Magagnin V, Bassani T, Tobaldini E et al (2011) Causal relationships between heart period and systolic arterial pressure during graded head-up tilt. *Am J Physiol* 300:R378–R386
25. Baccala LA, Sameshima K (2001) Partial directed coherence: a new concept in neural structure determination. *Biol Cybern* 84:463–474
26. Kaminski M, Ding M, Truccolo WA, Bressler S (2001) Evaluating causal relations in neural systems: Granger causality, directed transfer function and statistical assessment of significance. *Biol Cybern* 85:145–157
27. Porta A, Furlan R, Rimoldi O, Pagani M, Malliani A, van de Borne P (2002) Quantifying the strength of linear causal coupling in closed loop interacting cardiovascular variability series. *Biol Cybern* 86:241–251
28. Nollo G, Faes L, Porta A, Antolini R, Ravelli F (2005) Exploring directionality in spontaneous heart period and systolic pressure variability interactions in humans: implications in the evaluation of baroreflex gain. *Am J Physiol* 288:H1777–H1785
29. Eichler M (2006) On the evaluation of information flow in multivariate systems by the directed transfer function. *Biol Cybern* 94:469–482
30. Schelter B, Timmer J, Eichler M (2009) Assessing the strength of directed influences among neural signals using renormalized partial directed coherence. *J Neurosci Methods* 179:121–130
31. Chicharro D (2011) On the spectral formulation of Granger causality. *Biol Cybern* 105:331–347
32. Faes L, Erla S, Porta A, Nollo G (2013) A framework for assessing frequency domain causality in physiological time series with instantaneous effects. *Phil Trans R Soc A* 371:20110618
33. Pernice R, Sparacino L, Bari V, Gelpi F, Cairo B, Mijatovic G et al (2022) Spectral decomposition of cerebrovascular and cardiovascular interactions in patients prone to postural syncope and healthy controls. *Auton Neurosci: Basic Clin* 242:103021
34. De Boer RW, Karemaker JM, Strackee J (1987) Hemodynamic fluctuations and baroreflex sensitivity in humans: a beat-to-beat model. *Am J Physiol* 253:H680–H689
35. Baselli G, Cerutti S, Badilini F, Biancardi L, Porta A, Pagani M et al (1994) Model for the assessment of heart period and arterial pressure variability interactions and of respiration influences. *Med Biol Eng Comput* 32:143–152
36. Claassen JAHR, Meel-van den Abeelen ASS, Simpson DM, Panerai RB on behalf of the International Cerebral Autoregulation Research Network (CARNet) (2016) Transfer function analysis of dynamic cerebral autoregulation: a white paper from the International Cerebral Autoregulation Research Network. *J Cereb Blood Flow Metab* 36:665–680
37. Barnett L, Barrett AB, Seth AK (2009) Granger causality and transfer entropy are equivalent for Gaussian variables. *Phys Rev Lett* 103:238701
38. Baselli G, Porta A, Rimoldi O, Pagani M, Cerutti S (1997) Spectral decomposition in multichannel recordings based on multi-variate parametric identification. *IEEE Trans Biomed Eng* 44:1092–1101
39. Faes L, Porta A, Rossato G, Adami A, Tonon D, Corica A et al (2013) Investigating the mechanisms of cardiovascular and cerebrovascular regulation in orthostatic syncope through an information decomposition strategy. *Auton Neurosci: Basic Clin* 178:76–82
40. Bari V, Marchi A, De Maria B, Rossato G, Nollo G, Faes L et al (2016) Nonlinear effects of respiration on the crosstalk between cardiovascular and cerebrovascular control systems. *Phil Trans R Soc A* 374:20150179
41. Aaslid R, Markwalder TM, Nornes H (1982) Noninvasive transcranial Doppler ultrasound recording of flow velocity in basal cerebral arteries. *J Neurosurg* 57:769–774
42. Task Force of the European Society of Cardiology and the North American Society of Pacing and Electrophysiology (1996) Heart rate variability: standards of measurement, physiological interpretation and clinical use. *Circulation* 93:1043–1065
43. Magagnin V, Bassani T, Bari V, Turiel M, Maestri R, Pinna GD et al (2011) Non-stationarities significantly distort short-term spectral, symbolic and entropy heart rate variability indexes. *Physiol Meas* 32:1775–1786

44. Gelpi F, Bari V, Cairo B, De Maria B, Tonon D, Rossato G et al (2022) Dynamic cerebrovascular autoregulation in patients prone to postural syncope: comparison of techniques assessing the autoregulation index from spontaneous variability series. *Auton Neurosci: Basic Clin* 237:102920
45. Porta A, Cairo B, Bari V, Gelpi F, De Maria B, Colombo R (2023) Model-based spectral causality of cardiovascular variability interactions during head-down tilt. *Physiol Meas* 44:054001
46. Akaike H (1974) A new look at the statistical novel identification. *IEEE Trans Autom Control* 19:716–723
47. Vaini E, Bari V, Fantinato A, Pistuddi V, Cairo B, De Maria B et al (2019) Causality analysis reveals the link between cerebrovascular control and acute kidney dysfunction after coronary artery bypass grafting. *Physiol Meas* 40:064006
48. Schreiber T, Schmitz A (1996) Improved surrogate data for non-linearity tests. *Phys Rev Lett* 77:635–638
49. Palus M (1997) Detecting phase synchronisation in noisy systems. *Phys Lett A* 235:341–351
50. Berger RD, Saul JP, Cohen RJ (1989) Transfer function analysis of autonomic regulation I. Canine atrial rate response. *Am J Physiol* 256:H143–H152
51. Saul JP, Berger RD, Chen MH, Cohen RJ (1989) Transfer function analysis of autonomic regulation II Respiratory sinus arrhythmia. *Am J Physiol* 256:H153–H161
52. Chen X, Mukkamala R (2008) Selective quantification of the cardiac sympathetic and parasympathetic nervous systems by multiresolution analysis of cardiorespiratory variability. *Am J Physiol* 294:H362–H371
53. Stauss HM, Anderson EA, Hayness WG, Kregel KC (1998) Frequency response characteristics of sympathetically mediated vasomotor waves in humans. *Am J Physiol* 274:H1277–H1283
54. Lewis ME, Al-Khalidi AH, Bonser RS, Clutton-Brock T, Morton D, Paterson D et al (2001) Vagus nerve stimulation decreases left ventricular contractility in vivo in the human and pig heart. *J Physiol* 534(2):547–552
55. Zhang R, Zuckerman JH, Giller CA, Levine BD (1998) Transfer function analysis of dynamic cerebral autoregulation in humans. *Am J Physiol* 274:H233–H241
56. Cushing H (1902) Some experimental and clinical observations concerning states of increased intracranial tension. *Am J Med Sci* 124:375–400
57. Yana K, Saul JP, Berger RD, Perrott MH, Cohen RJ (1993) A time domain approach for the fluctuation analysis of heart rate related to instantaneous lung volume. *IEEE Trans Biomed Eng* 40:74–81
58. Perrott MH, Cohen RJ (1996) An efficient approach to ARMA modeling of biological systems with multiple inputs and delays. *IEEE Trans Biomed Eng* 43:1–14
59. Patton DJ, Triedman JK, Perrott MH, Vidian AA, Saul JP (1996) Baroreflex gain: characterization using autoregressive moving average analysis. *Am J Physiol* 270:H1240–H1249
60. Mullen TJ, Appel ML, Mukkamala R, Mathias JM, Cohen RJ (1997) System identification of closed loop cardiovascular control: effects of posture and autonomic blockade. *Am J Physiol* 272:H448–H461
61. Faes L, Porta A, Cucino R, Cerutti S, Antolini R, Nollo G (2004) Causal transfer function analysis to describe closed loop interactions between cardiovascular and cardiorespiratory variability signals. *Biol Cybern* 90:390–399
62. Porta A, Bari V, Bassani T, Marchi A, Pistuddi V, Ranucci M (2013) Model-based causal closed loop approach to the estimate of baroreflex sensitivity during propofol anesthesia in patients undergoing coronary artery bypass graft. *J Appl Physiol* 115:1032–1042
63. Panerai RB, Dawson SL, Potter JF (1999) Linear and nonlinear analysis of human dynamic cerebral autoregulation. *Am J Physiol* 277:H1089–H1099
64. Simpson DM, Panerai RB, Evans DH, Naylor AR (2001) A parametric approach to measuring cerebral blood flow autoregulation from spontaneous variations in blood pressure. *Ann Biomed Eng* 29:18–25
65. Eckberg DL (2003) The human respiratory gate. *J Physiol* 548:339–352
66. Yildiz S, Thyagaraj S, Jin N, Zhong X, Soroush Pahlavian H, Martin BA et al (2017) Quantifying the influence of respiration and cardiac pulsations on cerebrospinal fluid dynamics using real-time phase-contrast MRI. *J Magn Reson Imaging* 46:431–439
67. Faes L, Nollo G, Porta A (2013) Mechanisms of causal interaction between short-term RR interval and systolic arterial pressure oscillations during orthostatic challenge. *J Appl Physiol* 114:1657–1667
68. Giller CA (1990) The frequency-dependent behavior of cerebral autoregulation. *Neurosurgery* 27:362–368
69. Montano N, Gneccchi-Ruscione T, Porta A, Lombardi F, Pagani M, Malliani A (1994) Power spectrum analysis of heart rate variability to assess changes in sympatho-vagal balance during graded orthostatic tilt. *Circulation* 90:1826–1831
70. Furlan R, Porta A, Costa F, Tank J, Baker L, Schiavi R et al (2000) Oscillatory patterns in sympathetic neural discharge and cardiovascular variables during orthostatic stimulus. *Circulation* 101:886–892
71. Levine BD, Giller CA, Lane LD, Buckley JC, Blomqvist CG (1994) Cerebral versus systemic hemodynamics during graded orthostatic stress in humans. *Circulation* 90:298–306
72. Carey BJ, Manktelow BN, Panerai RB, Potter JF (2001) Cerebral autoregulatory responses to head-up tilt in normal subjects and patients with recurrent vasovagal syncope. *Circulation* 104:898–902
73. Grubb BP, Gerard G, Roush K, Temesy-Armos P, Montford P, Elliott L et al (1991) Cerebral vasoconstriction during head-upright tilt-induced vasovagal syncope: a paradoxical and unexpected response. *Circulation* 84:1157–1164
74. Tzeng YC, MacRae BA, Ainslie PN, Chan GSH (2014) Fundamental relationships between blood pressure and cerebral blood flow in humans. *J Appl Physiol* 117:1037–1048
75. Laitinen T, Niskanen L, Geelen G, Lämsimies E, Hartikainen J (2004) Age dependency of cardiovascular autonomic responses to head-up tilt in healthy subjects. *J Appl Physiol* 96:2333–2340
76. Milan-Mattos JC, Porta A, Perseguini NM, Minatel V, Rehder-Santos P, Takahashi ACM et al (2018) Influence of age and gender on the phase and strength of the relation between heart period and systolic blood pressure spontaneous fluctuations. *J Appl Physiol* 124:791–804
77. Sachse C, Trozic I, Brix B, Roessler A, Goswami N (2019) Sex differences in cardiovascular responses to orthostatic challenge in healthy older persons: a pilot study. *Physiol Int* 106:236–249
78. Reulecke S, Charleston-Villalobos S, Voss A, González-Camarena R, González-Hermosillo J, Gaitán-González MJ et al (2016) Men and women should be separately investigated in studies of orthostatic challenge due to different gender-related dynamics of autonomic response. *Physiol Meas* 37:314–332
79. Rosenberg AJ, Kay VL, Anderson GK, Luu M-L, Barnes HJ, Sprick JD et al (2022) The reciprocal relationship between cardiac baroreceptor sensitivity and cerebral autoregulation during simulated hemorrhage in humans. *Auton Neurosci: Basic Clin* 241:103007
80. Gelpi F, Bari V, Cairo B, De Maria B, Tonon D, Rossato G, et al (2021) Correlation between baroreflex sensitivity and cerebral autoregulation index in healthy subjects. *Comput Cardiol* 48. <https://doi.org/10.23919/CinC53138.2021.9662726>.
81. Marchi A, Bari V, De Maria B, Esler M, Lambert E, Baumert M et al (2016) Simultaneous characterization of sympathetic and

cardiac arms of the baroreflex through sequence techniques during incremental head-up tilt. *Front Physiol* 7:438

82. Porta A, Bari V, De Maria B, Cairo B, Vaini E, Malacarne M et al (2018) Peripheral resistance baroreflex during incremental bicycle ergometer exercise: characterization and correlation with cardiac baroreflex. *Front Physiol* 9:688
83. Reyes del Paso GA, de la Coba P, Martín-Vazquez M, Thayer JF (2017) Time domain measurement of the vascular and myocardial branches of the baroreflex: a study in physically active versus sedentary individuals. *Psychophysiology* 54:1528–1540
84. Yasumasu T, Abe H, Oginosawa Y, Takahara K, Nakashima Y (2005) Assessment of cardiac baroreflex function during fixed atrioventricular pacing using baroreceptor-stroke volume reflex sensitivity. *J Cardiovasc Electrophysiol* 16:727–731
85. Vaschillo EG, Vaschillo B, Buckman JF, Pandina RJ, Bates ME (2012) Measurement of vascular tone and stroke volume baroreflex gain. *Psychophysiology* 49:193–197
86. Casadei B, Meyer TE, Coats AJ, Conway J, Sleight P (1992) Baroreflex control of stroke volume in man: an effect mediated by the vagus. *J Physiol* 448:539–550
87. Sadeghian F, Divsalar DN, Fadil R, Tavakolian K, Blaber AP (2022) Canadian aging and inactivity study: spaceflight-inspired exercises during head-down tilt bedrest blunted reductions in muscle-pump but not cardiac baroreflex in older persons. *Front Physiol* 13:943630
88. Verma AK, Garg A, Xu D, Bruner M, Fazel-Rezai R, Blaber AP et al (2017) Skeletal muscle pump drives control of cardiovascular and postural systems. *Scient Rep* 7:45301
89. Fadil R, Huether AXA, Verma AK, Brunner R, Blaber AP, Lou J-S et al (2022) Effect of Parkinson's disease on cardio-postural coupling during orthostatic challenge. *Front Physiol* 13:863877
90. Wieling W, van Dijk N, Thijs RD, de Lange FJ, Paul Krediet CT, Halliwill JR (2015) Physical countermeasures to increase orthostatic tolerance. *J Intern Med* 277:69–82
91. Fadil R, Verma AK, Sadeghian F, Blaber AP, Tavakolian K (2023) Cardio-respiratory interactions in response to lower-body negative pressure. *Physiol. Meas* 44:025005
92. de Abreu RM, Catai AM, Cairo B, Rehder-Santos P, Dionisete da Silva CD, De Favari SE et al (2020) A transfer entropy approach for the assessment of the impact of inspiratory muscle training on the cardiorespiratory coupling of amateur cyclists. *Front Physiol* 11:134

Publisher's note Springer Nature remains neutral with regard to jurisdictional claims in published maps and institutional affiliations.



Alberto Porta received an MS degree in Electronic Engineering and a PhD degree in Biomedical Engineering from the Politecnico di Milano, Milan, Italy, in 1989 and 1999, respectively. Since 1999, he has been with the University of Milan, Milan, Italy, where he is currently a full professor in Biomedical Engineering. His current H-index is 64 (source: Scopus).



Francesca Gelpi received the MS degree in Biomedical Engineering from KuLeuven, Leuven, Belgium in 2017 and she is currently a PhD student in Translational Medicine at University of Milan, Milan, Italy. Her current H-index is 5 (source: Scopus).



Vlasta Bari received an MS and PhD degree in Bioengineering from Politecnico di Milano, Milan, Italy in 2010 and 2014, respectively. Since 2016, she has been biomedical engineer and researcher at IRCCS Policlinico San Donato, Milan, Italy. She is currently assistant professor at the University of Milan, Milan, Italy since 2022. Her current H-index is 23 (source: Scopus).



Beatrice Cairo received an MS degree in Biomedical Engineering from Politecnico di Milano, Milan, Italy, in 2010 and a PhD degree in Integrative Biomedical Research from the University of Milan, Milan, Italy, in 2021. She is currently a Research Fellow at the University of Milan, Milan, Italy. Her current H-index is 12 (source: Scopus).



Beatrice De Maria received the MS degree in Biomedical Engineering and the PhD degree in Biomedical Engineering from Politecnico di Milano, Milan, Italy, in 2014 and 2018, respectively. Since 2014, she has been with the IRCCS Istituti Clinici Scientifici Maugeri. Her current H-index is 16 (source: Scopus).



Davide Tonon received a degree in Neurophysiopathological Techniques at the University of Udine, Italy, in 2008. Since 2008, he works at the Neurology Department of IRCCS Sacro Cuore Don Calabria, Verona, Italy, and since 2013, he is the Coordinator of Neurophysiopathology Technicians of the Sleep Clinic in the same Hospital. He is part of the teaching staff of Clinical Neurophysiology Technology Program at the University of Padova. His current H-index is 5 (source: Scopus).



Luca Faes is a full Professor of Biomedical Engineering at the University of Palermo, Italy. He has previously been with the Department of Physics of the University of Trento, Italy, and a visiting scientist at the State University of New York, Worcester Polytechnic Institute, University of Gent, University of Minas Gerais, and Boston University. He co-authored eight book chapters and more than 250 peer-reviewed publications, receiving > 6000 citations (H-index: 46; source: Scholar).



Gianluca Rossato received an MD degree in Medicine and completed the Residency in Neurology at the University of Verona, Italy, in 1999 and 2004 respectively. Since 2013, he is the Founder and Director of the Sleep Clinic in the Neurology Department of IRCCS Sacro Cuore Don Calabria, Verona, Italy. His current H-index is 8 (source: Scopus).